Chemical Science

Accepted Manuscript

This article can be cited before page numbers have been issued, to do this please use: I. V. Koshelev, A. N. Selikhov, A. Cherkasov, R. R. Aysin and A. A. Trifonov, *Chem. Sci.*, 2026, DOI: 10.1039/D6SC03562K.

ROYAL SOCIETY OF CHEMISTRY

rsc.li/chemical-science

View Article Online
DOI: 10.1039/D6SC03562K

ARTICLE

Highly regio- and *E*-stereoselective C=C bond transposition catalyzed by tris(benzhydryl) sodium calciate. Proof of synergy: one metal is good, but two are better

Received 00th January 20xx,
Accepted 00th January 20xx

DOI: 10.1039/x0xx00000x

Ivan V. Koshelev,[a] Alexander N. Selikhov,[a]* Anton V. Cherkasov,[a] Rinat R. Aysin,[b] and Alexander A. Trifonov[a, b]*

Here, we report the synthesis of tris(benzhydryl) sodium calciate {[(*p*-*t*Bu-C_6H_4)$_2$CH]$_3$Ca}Na (**3**) featuring the structure of a base-free contact ion pair. Catalytic amounts (2 mol%) of **3** containing earth-abundant and biogenic s-metals combined with pyrrolidine as a co-catalyst (H^+-donor) enable efficient regio- and stereocontrollable C=C bond transposition at ambient temperature. Allyl- and homoallylbenzenes undergo thermodynamically controlled isomerization to afford prop-1-en-1-yl- and but-1-en-1-ylbenzenes with *E*-stereoselectivity up to 98%. The exceptionally regioselective isomerization of terminal α-olefins (1-hexene - 1-decene) to internal 2-olefins catalyzed by **3**/pyrrolidine (23 °C) to yield a mixture of *E*- and *Z*-isomers proved to be kinetically controlled. Mechanistic investigations revealed that these processes involve the *in situ* formation of a heterobimetallic amide complex, which catalyzes olefin isomerization through a methylene group deprotonation followed by a metallotropic rearrangement. The DFT calculations elucidate the mechanism of the catalytic cycle and explain *E*/*Z*-selectivity in terms of kinetic and thermodynamic controls. In particular, QTAIM analysis revealed coordination of allylic intermediates to both metallic centers and therefore defined a synergetic effect of the heterobimetallic catalyst

Introduction

The olefin functional group is one of the most important and frequently encountered structural motifs of compounds widely used in the pharmaceutical, agrochemical, perfumery, food industries, as well as the chemistry of functional materials.[1] Its formation in highly regio- and stereoselective manner is of great importance, since geometry ultimately determines the function. Among the methods providing access to internal olefins, double bond migration along with olefin metathesis[2i-j] and acetylenes semihydrogenation[2k-l] is a fundamental valuable approach characterized by 100% atom economy, which is of particular importance for the synthesis of internal olefins featuring a defined stereoconfiguration of the C=C bond.[2] Terminal olefins are readily available through ethylene oligomerization and proven methods of introducing the allyl group into aromatic core, so the strategy of their catalytic conversion to internal analogues represents a promising approach. However, control of stereoselectivity and regioselectivity remains challenging, especially when performing isomerization to non-activated positions.

Over the years, the transition metal-catalyzed positional isomerization of alkenes under mild reaction conditions has been greatly developed and made it possible to implement a process with high regio- and *E*/*Z*-stereocontrol. To date, transition-metal catalyzed olefin isomerization focused primarily on three distinct mechanisms (Fig. 1, A). (1) The most common metal-hydride protocol[2a] is implemented using derivatives of transition both precious and more abundant metals, including Pd,[3] Ir,[4] Ru,[5] Co,[6] Fe,[7] Mo,[8] Mn,[9] Ni,[10] Cr.[11] (2) The less-documented π-allyl mechanism consists in oxidative addition of low-valent metal to an olefin with subsequent reductive elimination through allyl intermediate.[12] (3) Metal-radical induced 1,3-H atom relocation mechanism.[13] In addition, visible-light-driven and electrochemical approaches to isomerization of terminal olefins have been reported (Fig. 1, B).[14] In addition, the field of photochemical contra-thermodynamic positional isomerization has been actively developing recently.[14c, 15]

However, despite the remarkable achievements in transition-metal catalysis, their significant polar functional group (CN, COR, COOH, NO_2, etc.) tolerance,[3,4c,7a,10] a key challenge in this arena that limits the industrial relevance of these systems is the use of unrecyclable precious metal catalysts and/or stoichiometric additives. Moreover, late transition metals are often toxic and require a sophisticated ligand environment, which limits their potential for pharmaceutical applications.

[a] G.A. Razuvaev Institute of Organometallic Chemistry of Russian Academy of Sciences, 49 Tropinina str., 603950, Nizhny Novgorod, Russia
[b] A.N. Nesmeyanov Institute of Organoelement Compounds of Russian Academy of Sciences, 28 build. 1, Vavilova str., 119334, Moscow, Russia
[c] † Footnotes relating to the title and/or authors should appear here.

View Article Online
DOI: 10.1039/D6SC03562K

ARTICLE

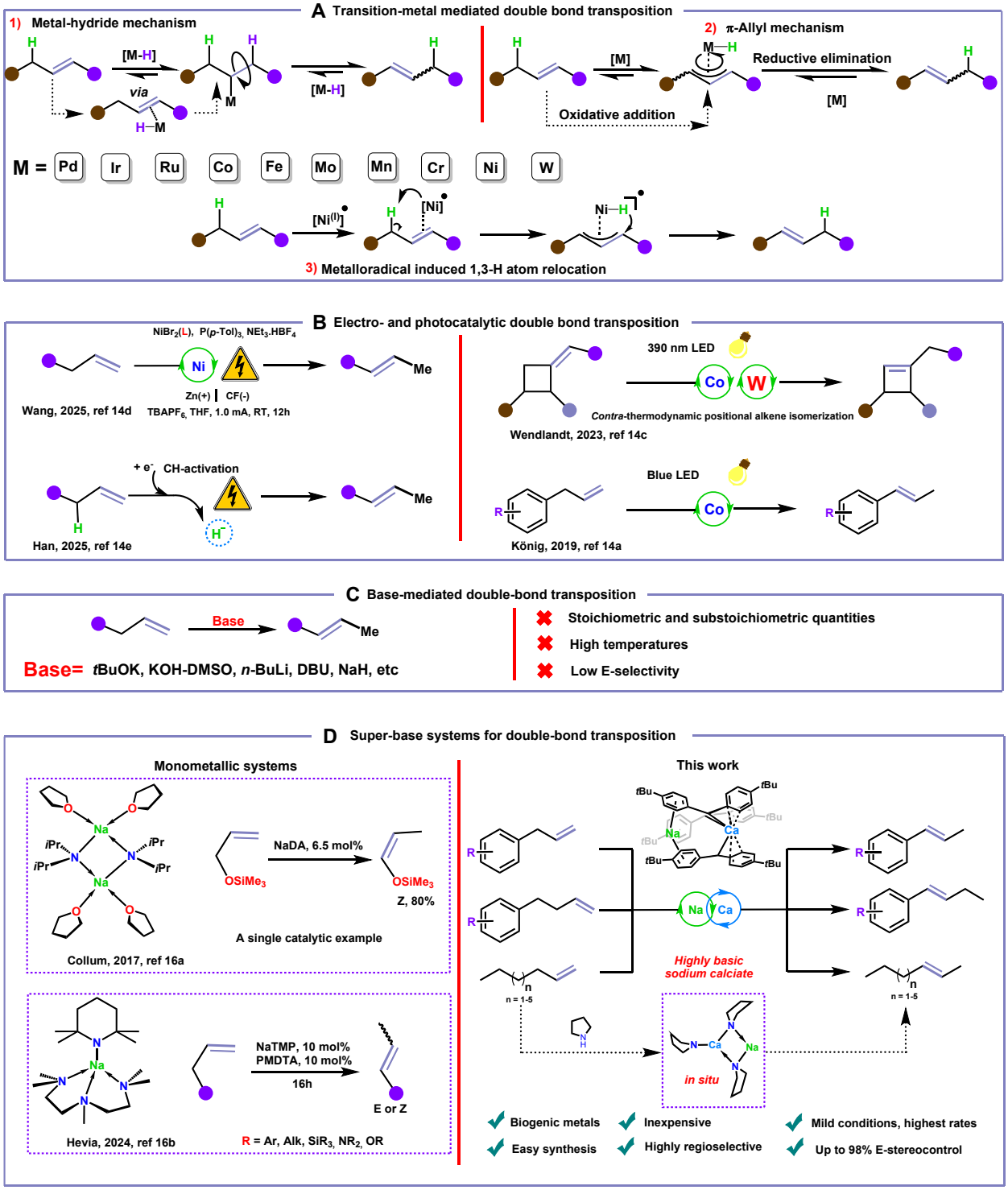

Fig. 1 Alkene isomerizations. **A**: transition-metal complex-mediated olefin transpositions; **B**: electro- and photocatalytic double-bond transposition; **C**: Stoichiometric base-mediated double-bond transposition; **D**: super-base systems for catalytic double-bond transposition.

View Article Online
DOI: 10.1039/D6SC03562K

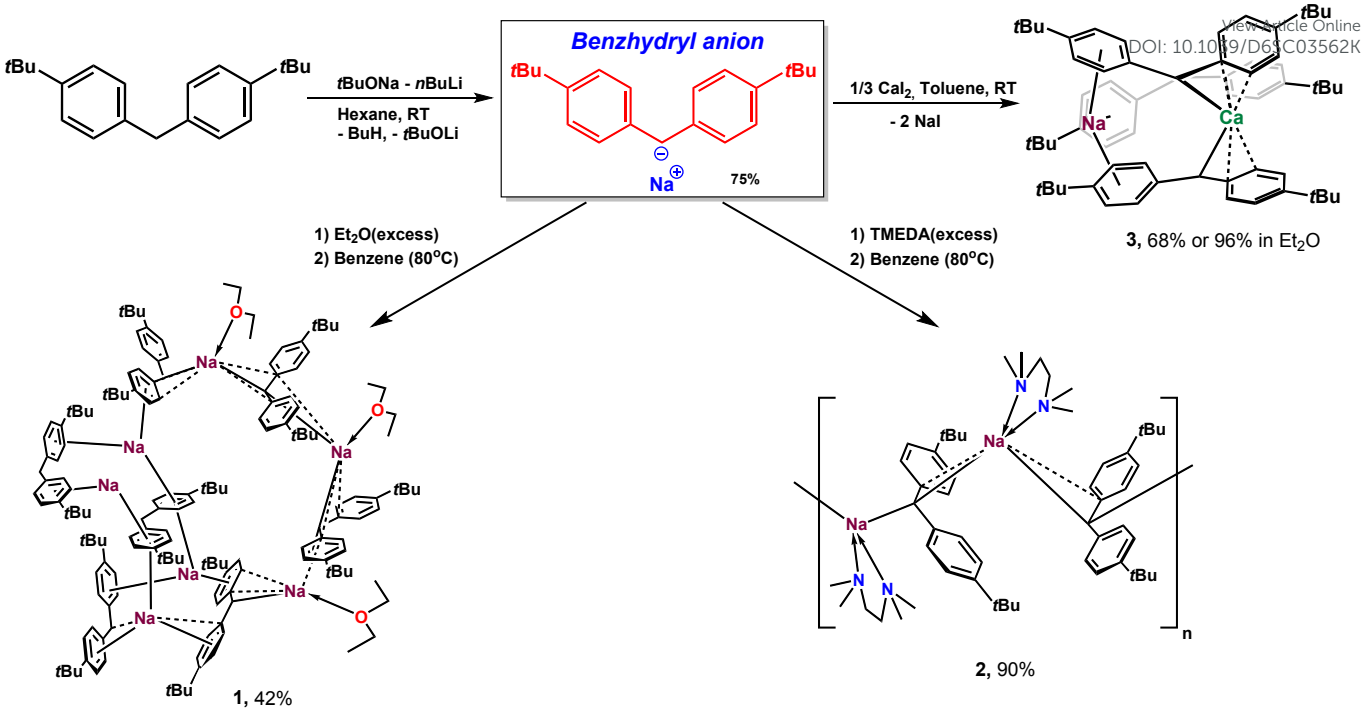

Scheme 1. Synthesis of complexes **1**-**3**.

Therefore, the obvious economic constraints caused by the limited availability, sensitivity and toxicity of precious metal complexes are causing growing interest in the search for new isomerization catalysts that are ideally earth-abundant and biogenic.

Since the 1960s, base-mediated isomerization has become widely used in laboratory practice (Fig. 1, C).[2c, 16] However, the widespread base-mediated protocol requires stoichiometric and substoichiometric amounts of bases (*t*BuOK, KOH-DMSO, etc), polar solvents, and very harsh reaction conditions with temperatures up to 200 °C.

This has a negative impact on regio- and especially stereo-selectivity, and is also incompatible with many functional groups. Nevertheless, increasing the basicity of the system through a rational selection of metals and ligands can enable catalytic isomerization under mild conditions.[1, 17]

Indeed, in 2017, Collum demonstrated that super-base NaDA (DA=*N,N*-diisopropylamide) can promote the isomerization of alkenes, but only one example of isomerization in the catalytic regime was described in the work (Fig. 1, D).[17a] The monometallic super-basic system NaTMP-PMDTA (TMP = 2,2,6,6-tetramethylpiperidine) developed by Hevia allowed for the isomerization of allylbenzenes, allylamides and O-allyl ethers with a high degree of stereocontrol. The nature of the metal, the amide anion, and the neutral base proved to be dramatically affecting the conversions and the *E*/*Z* ratio.[17b]

To date, most of the catalysts for double bond transposition are presented by monometallic complexes, only a handful of studies are devoted to cooperative catalysis.[4b, 7c, 18]

The interest in heterobimetallic complexes of s-block elements is inspired by their distinctive reactivity enhancement compared to that of the homometallic analogues;[19] however, their potential in catalysis of double bond migration has not yet been explored.

Recently we successfully introduced into the organometallic chemistry of rare- and alkaline earth metals the new bulky benzhydryl ligand $[(p\text{-}t\text{BuC}_6\text{H}_4)_2\text{CH}]^-$, which proved to be a unique platform for the synthesis of isolable, highly reactive and exceptionally thermally stable complexes.[20] In particular, in 2023 we reported unprecedented catalytic activity and regioselectivity of bimetallic *ate*-complex $\{[(p\text{-}t\text{BuC}_6\text{H}_4)_2\text{CH}]_3\text{Ca}\}\text{K}$ in intermolecular olefin hydroamination allowing to involve into the reaction a broad scope of substrates including ethylene, internal olefins, and a variety of primary and secondary amines.[21] The synergistic effect of the presence of two different metals was convincingly evidenced.

Results and discussion

Synthesis and structure of heterobimetallic complex 3

Keeping in mind exceptional catalytic activity of rare- and alkaline earth benzhydryl complexes in a variety of olefin transformations as well as super-basic character of calciate anion $\{[(p\text{-}t\text{BuC}_6\text{H}_4)_2\text{CH}]_3\text{Ca}\}^-$ we proposed to apply a potential of bimetallic complexes in the development of a new efficient approach to olefin isomerization. Hence, readily accessible complex $\{[(p\text{-}t\text{BuC}_6\text{H}_4)_2\text{CH}]_3\text{Ca}\}\text{Na}$ containing cheap biogenic metals was synthesized.

For the synthesis of **3** the sodium derivative $[(p\text{-}t\text{BuC}_6\text{H}_4)_2\text{CH}]\text{Na}$ was obtained by the Lochman-Schlosser reaction of 4,4'-di-*tert*-butyl-diphenylmethane with *n*BuLi and *t*BuONa in 75% yield.[22] The treatment of Lewis base-free $[(p\text{-}t\text{BuC}_6\text{H}_4)_2\text{CH}]\text{Na}$ with excess Et_2O or TMEDA and subsequent

crystallization from hot benzene afford single crystals of **1** and **2** (Scheme 1). The X-ray structure and NMR spectra description of complexes **1-2** are given in ESI (figures S15, S16).

The salt metathesis reaction of CaI_2 with $[(p\text{-}t\text{Bu}C_6H_4)_2CH]Na$ (molar ratio 1:3, toluene, 23 °C, 2h) affords a Lewis base-free heterobimetallic complex $\{[(p\text{-}t\text{Bu}C_6H_4)_2CH]_3Ca\}Na$ (**3**). It is noteworthy, that this reaction leads to the formation of **3** regardless the molar ratio of reagents. However, the nature of the reaction solvent proved to be crucial for the reaction outcome. Thus, the reaction proceeds smoothly in arenes to form deep-red crystals of **3** in 68 % yield after recrystallization from toluene-hexane mixture (1:2). In aliphatic hydrocarbons the reaction does not occur due to the low solubility of starting reagents and the reaction product. Furthermore, the use of coordinating THF as a reaction medium provides the formation of a neutral bis(benzhydryl) species, which was isolated in a crystalline state as a TMEDA-adduct $[(p\text{-}t\text{Bu}C_6H_4)_2CH]_2Ca(TMEDA)$.[20a] The yield of **3** can be increased to 96% if the reaction is carried out in Et_2O (1 h, RT).

Once crystallized from toluene-hexane mixture **3** becomes poorly soluble in arenes. The ^1H and $^{13}C\{^1H\}$ NMR spectra of **3** were recorded in C_6D_6/THF-d_8 mixture (10:1) and present the single set of signals, indicating equivalence of benzhydryl ligands. In the ^1H NMR spectrum, the central methanide CH protons appear as a singlet with chemical shift of 4.10 ppm, which is almost identic to that of the related complex $\{[(p\text{-}t\text{Bu}C_6H_4)_2CH]_3Ca\}K$ (4.16 ppm).[21] The aromatic *meta*-CH protons give rise to a distinct doublet at 6.94 ppm, however *ortho*-CH protons are strongly broadened indicating the occurrence of dynamic processes (See SI, Fig. S11). Similar intramolecular dynamic was previously revealed for *tris*-benzhydryl complexes $[(p\text{-}t\text{Bu}C_6H_4)_2CH]_3Ln$ (Ln = Y, La).[20c] This behavior is attributed to the unsymmetric metal-ligand bonding featuring the presence of close contact of one of the *o*-CH protons with metal as evidenced by the single crystal X-ray diffraction study (SC XRD) (see below for details). Increasing the temperature to 333 K leads to a sharpening of the o-CH signals without changing the chemical shift (SI, Fig. S13), which is caused by the restoration of the averaged "symmetric" bonding mode. Unfortunately, low temperature studies in toluene-d_8 are impossible due to rapid complex crystallization from a saturated solution. Unfortunately, due to the dynamic processes in solution, it is not possible to record a high-quality ^1H DOSY NMR spectrum for complex **3**.[23]

Unlike the previously published benzyl lithium calciate $[(PhCH_2)_4CaLi_2(TMEDA)_2]$, the addition of THF does not result in immediate complex decomposition via ether cleavage and the enolate formation.[24] Instead, **3** demonstrated impressive stability in C_6D_6/THF-d_8 solution, showing no visible signs of decomposition for 72 h at RT. However, increasing the temperature to 70 °C leads to rapid decomposition of the complex ($t_{1/2}$ ≈ 48h), accompanied by the release of diphenylmethane $(p\text{-}t\text{Bu}C_6H_4)_2CH_2$ as the main product. High thermal stability and high reactivity of M-C bonds constitute a great advantage of benzhydryl complexes.

The single crystal X-ray diffraction study revealed that complex **3** is heterobimetallic, base-free and adopts a rather unusual structure of a contact ion pair (Fig. 2). In contrast to the previously described Ca/K *ate*-complex,[21] in **3** an asymmetric binding of three benzhydryl ligands to the metals is observed. Two benzhydryl ligands coordinate to the Ca(II) ion in a η^3-fashion *via* a covalent bond with the methanide carbon (2.544(3), 2.614(3) Å) and non-covalent interactions with the *ipso*- (2.688(2), 2.690(3) Å) and *ortho*- (2.688(3), 2.757(3) Å) carbons of one phenyl ring. The second phenyl rings of two benzhydryl fragments encapsulate Na^+ cation in η^4- and η^6-modes with Na…C distances falling within the range 2.700(3)-3.172(3) Å. One phenyl ring is coordinated rather symmetrically (Na…C 2.824(3)-2.980(3) Å), while for the second one two Na…C distances (3.157(3), 3.172(3) Å) are noticeably longer than the others (2.700(3)-2.982(3) Å).

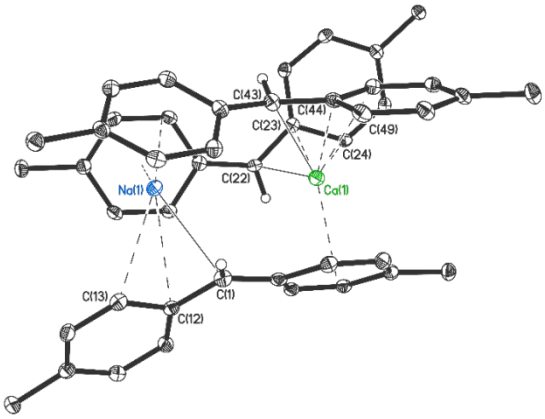

Figure 2. Molecular structure of **3**. Thermal ellipsoids are given at a 30% probability level. Methyl groups of *tert*-butyl substituents, and all hydrogen atoms (except methanide groups) are omitted for clarity.

Interestingly, despite of the difference of Na and K ion sizes, the Ca-$CH_{benzhydryl}$ bond distances in **3** are comparable to those in the related complex $\{[(p\text{-}t\text{Bu}C_6H_4)_2CH]_3Ca\}K$ (2.555(6)-2.603(6) Å) and bis(benzhydryl) $[(p\text{-}t\text{Bu}C_6H_4)_2CH]_2Ca(TMEDA)$ (2.545(2)- 2.647(2) Å)[20a] complexes. The coordination of the third benzhydryl ligand is inverted compared to that of two others. It is η^3-coordinated with the Na ion via the methanide carbon (Na–$CH_{benzhydryl}$ (2.672(3) Å), *ipso* (2.820(3) Å) and *ortho* (2.868(3) Å) phenyl carbons, while the Ca(II) ion does not interact with the methanide carbon. Instead, it is coordinated by phenyl ring in η^6-mode (Ca…C 2.691(3)-2.897(3) Å).

Catalytic activity of complex 3 in olefin isomerization

The catalyst screening was carried out on a model reaction of isomerization of the ubiquitous allylbenzene **4a** (Table 1, SI Fig. S58-S66). Complex **3** in THF solution (2 mol %, 23 °C) in the presence of pyrrolidine (15 mol %) as a proton source demonstrated unprecedented activity (Entry 1). The reaction was complete in less than 5 minutes and afforded prop-1-en-1-ylbenzene in 98% yield and 97% *E*-stereoselectivity. In comparison with the previously published isomerizations enabled by Fe,[7a,b] Pd,[3a] Ir,[4c] Co,[6a,b] and Sc catalysts,[17c] requiring prolonged heating, complex **3** catalyzes the transformation under very mild conditions. Moreover, the combination of a

pair of Earth-abundant biogenic metals and an accessible non-toxic benzhydryl anion makes the complex suitable for the isomerization of unsaturated substrates and the synthesis of molecules of interest for pharmaceutical applications. The nature of the H^+-source has a strong influence on the efficiency of isomerization. Thus, the use of a bulkier secondary amine – iPr$_2$NH as a co-catalyst, as well as any other secondary amines of comparable pKa (piperidine, diethylamine etc.)[25] does not reduce the activity of complex **3** (Entry 2). However, primary tBuNH$_2$ significantly dropped the reaction rate, and it took 24 h to reach 74% yield (entry 3).

Table 1 Optimization of the Reaction Conditions[a]

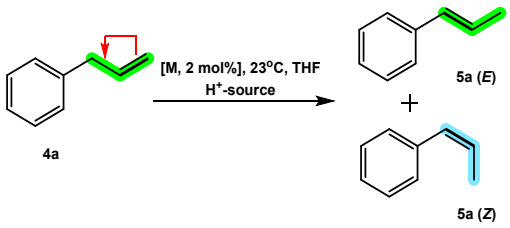

Entry	Catalyst	H^+-source	Time	Yield of **5a** %[b] (*E*:*Z*)[c]
1	**3**	**$(CH_2)_4NH$**	**<5 min**	**98 (97:3)**
2	**3**	***i*Pr$_2$NH**	**<5 min**	**98 (97:3)**
3[d]	**3**	***t*BuNH$_2$**	**24h**	**75 (90:10)**
4	**3**	**2-picoline**	**24h**	**24**
5	**3**	**–**	**24h**	**trace**
6[d]	**3**	**$(CH_2)_4NH$**	**<5 min**	**90 (98:2)**
7[e]	**1**	**$(CH_2)_4NH$**	**1 h**	**15**
8[e]	**2**	**$(CH_2)_4NH$**	**1 h**	**18**
9	**L$_2$Ca(TMEDA)**[f]	**$(CH_2)_4NH$**	**10h**	**98 (96:4)**
10	**LK**[f]	**$(CH_2)_4NH$**	**10h**	**70**
11	**L$_3$CaK**[f]	**$(CH_2)_4NH$**	**10 min**	**98**
12	**NaHMDS**	**–**	**24h**	**trace**

[a]Reaction conditions: **4a** (1.5 mmol), 15 mol % of H^+-source (0.2 mmol), THF (0.5 mL), 2 mol % of the metal complex in a sealed NMR tube. [b]The total yields of stereoisomers after flash distillation or flash column chromatography are given. [c]Ratios determined by ^{1}H NMR analysis. [d]Benzene was used as a solvent (0.5 ml). [e] 10 mol % of the metal complex in a sealed NMR tube was used. [f] L = diphenylmethanide anion (p-tBuC$_6$H$_4$)$_2$CH$^-$.

Stereocontrol of the reaction also suffers when tBuNH$_2$ is applied, with a decrease of the *E*-isomer content to 90%. 2-Methylpyridine being a weak CH-acid is also capable to act as a proton donor, however the reaction proceeds sluggishly, achieving just 24% in 24 h. In the absence of a proton-containing co-catalyst, only traces of the isomerization product were observed within 24 h.

Switching from THF to the less polar solvent benzene did not lead to a noticeable change in the catalytic performance of the catalyst **3** (Entry 6). However, further experiments were carried out in THF. Interestingly, the previously described NaTMP (TMP = 2,2,6,6-tetramethylpiperidine) did not show any isomerization activity in THF solution.[17b] Complexes **1** and **2** alone have only negligible effectiveness in the absence of a calciate species. To achieve 15-18% yield of the isomerization product, an increase in the catalyst loading to 10 mol % is required. Moreover, upon reaching 18%, the reaction stops in both cases, and even an increase in temperature to 70 °C does not continue the process. In this case, the reaction is probably non-catalytic, and allylbenzene isomerized on substeichiometric amounts of base. Sodium superbase - NaTMP (10 mol%), can drive the reaction in a catalytic regime, as previously described by Hevia et al., but this requires the presence of PMDTA as a co-catalyst.[17b] Complex [(p-tBuC$_6$H$_4$)$_2$CH]$_2$Ca(TMEDA)[20a] alone without a sodium counterion catalyzes the isomerization of allylbenzene, however noticeably slower. The isomerization product was obtained in 98% yield in a much longer time (10 h) than in the case of **3**.

Noteworthy that the synthesis of the complex [(p-tBuC$_6$H$_4$)$_2$CH]$_2$Ca(TMEDA) is more difficult and laborious than **3**.[20a] NaHMDS was also evaluated alone and performed no activity even after 24 h; only trace amounts of the isomerization product were detected. Interestingly, [(p-tBuC$_6$H$_4$)$_2$CH]K in the presence of pyrrolidine catalyzes the conversion of alkylbenzene providing 70% conversion in 2 h at room temperature. However, the reaction is complicated by the formation of a large number of unidentifiable side products of allylbenzene transformation. In this case, activation of the conjugated aromatic system of the resulting propenylbenzene by potassium cation is possible,[26] which can further lead to dimerization, oligomerization, and the formation of cyclic structures.[27] The previously described potassium calciate [(p-tBuC$_6$H$_4$)$_2$CH]$_3$CaK also catalyzes isomerization in a highly efficient manner (98% yield in 10 min). However, the reaction does not stop at the *E*-propenylbenzene stage and its further conversion leads to unidentifiable products (Entry 11, SI, Fig. S66).

Thus, the best result was demonstrated by the heterobimetallic complex **3** in combination with pyrrolidine and the use of THF as a solvent. We identified pyrrolidine as the optimal co-catalyst. In the presence of iPr$_2$NH when isomerization is completed, *E*-propenylbenzene continues to transform into unidentified products. In this case, chemoselectivity is most likely kinetically controlled. Since the nitrogen lone pair in iPr$_2$NH is highly shielded, competition between the amine and the resulting *E*-propenylbenzene for the metal coordination sphere is possible,[26] making the insertion of a double bond likely. A range of allylbenzene substrates were evaluated under optimized reaction conditions to assess the scope and limitations of the isomerization process (Scheme 2). Unhindered alkyl-substituted allylbenzenes **4b-d** performed activity similar to that of **4a**, providing isomerization products in excellent yields and stereoselectivity.

View Article Online
DOI: 10.1039/D6SC03562K

ARTICLE

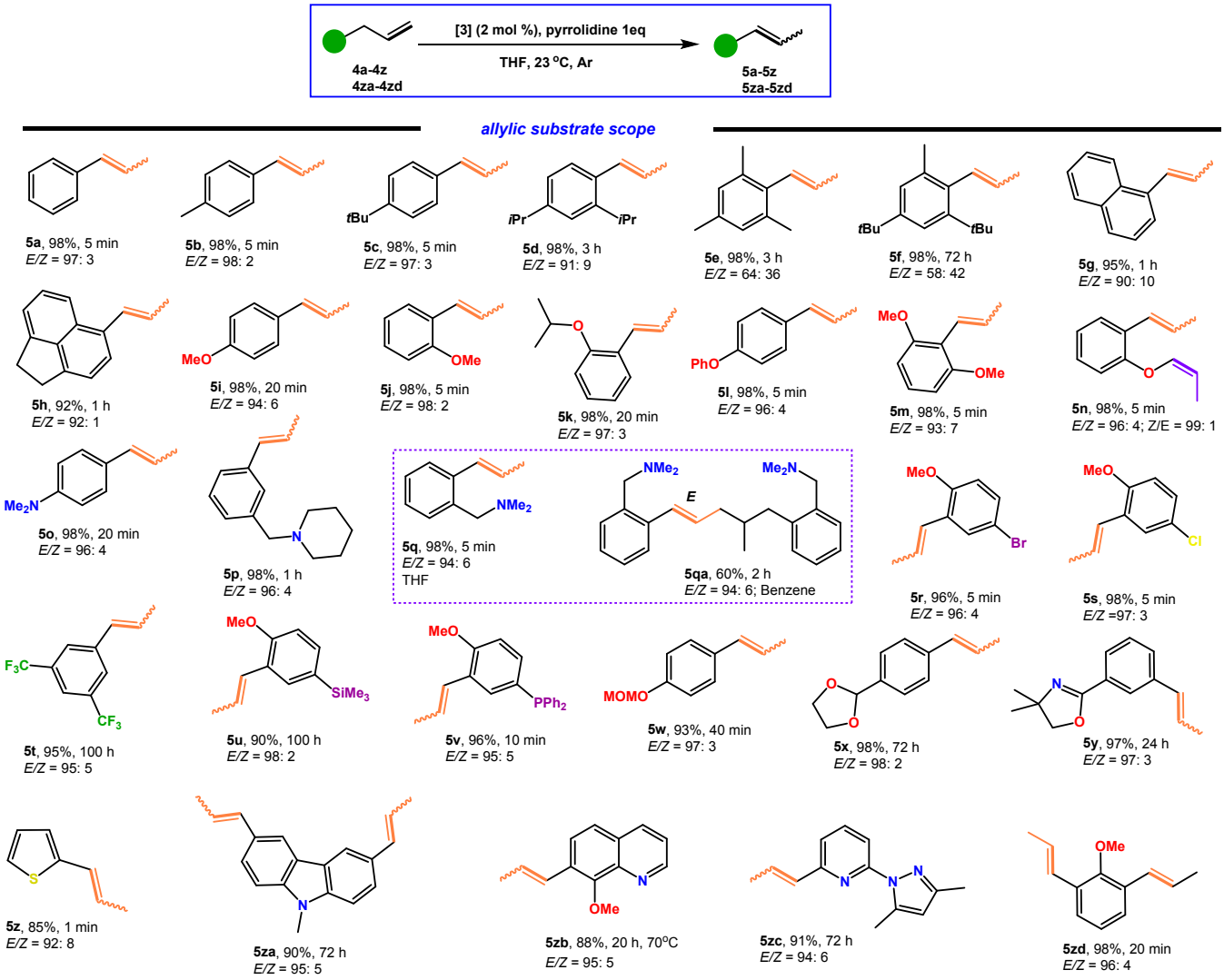

Scheme 2. Isomerization of allylbenzenes **4a-z, 4za, 4zb**, catalyzed by heterobimetallic complex **3**.

However, allylbenzenes **4e-f** with both *ortho*-positions blocked by *t*Bu and Me groups suffer from a much lower isomerization rate and stereoselectivity. Since the favorable formation of a conjugated planar allylic anion is the driving force of base-promoted isomerization, the predominant *E*-configuration of isomerization products **5a-d** is the result of thermodynamic control.[16] However, in the case of substrates **4e-f**, conjugation is disrupted due to the hampered rotation of the Ar fragments, preventing thermodynamic control (see below DFT for details). Allylic substrates with condensed aromatic substituents **4g** and **4h** in 5 min demonstrate 95-98% conversions, however *E*-selectivity reduced to 90 and 91% respectively.

Interestingly, despite of oxophilicity of Ca and Na cations, **3** tolerates alkyl- and aryl-protected oxygen functionality (**4i-m**) providing the formation of isomerized products **5i-m** in high yields and 98% *E*-stereoselectivity. For comparison: to transform **4i** into *trans*-anethole (**5i**), an important product for the pharmaceutical and fragrance industries, the prolong heating at 200 °C in the presence of excess aqueous NaOH or KOH allows for reaching just 56% conversion and an 82:18 *E/Z* ratio.[2c] Compared to *o,o*-dialkylsubstituted allylbenzenes *o,o*-dimetoxyallylbenzene (**4m**) readily undergoes a C=C bond transposition with excellent *E*-stereoselectivity (96%). In substrate **4n** regardless the different nature of allylic fragments for both fast isomerization (5 min) was

documented, yielding the product **5n** in which the allyl ether group isomerizes to give the *Z*-enol ether exclusively.

To demonstrate further the functional group compatibility of **3**, a series of amino group substituted allylbenzenes was evaluated. Thus, the introduction of the Me_2N group in *para*-position of aryl does not have a significant effect on the isomerization rate: 98% yield of the **5o** product was achieved in 20 min, albeit with high *E*-selectivity (96%). Conversion of the piperidine-substituted substrate (**4p**)[28] to the product requires more time (1 h, 98%), albeit it is obtained with excellent *E*-stereoselectivity (96 %). For *o*-N,N-dimethylaminomethyl substituted allylbenzene the reaction outcome was found to be dependent on the nature of the reaction media. In THF, the target isomerization occurs, achieving quantitative conversion of **4q** in 5 min (*E*/*Z* ratio 94:6%). While in benzene a regioselective a head-to-head dimerization occurs, yielding product **5qa** also with excellent *E*-selectivity (94%). Probably, in the absence of THF, the nitrogen directing group of **5q** facilitates intramolecular coordination of the double bond to the s-block metal in the catalytic intermediate, which ultimately promotes CH activation of the methyl group of the resulting *E*-propenylbenzene. Subsequently, a second *E*-propenylbenzene molecule **5q** is coordinated and inserted into the M-C bond, which is also facilitated by the presence of the directing amino group. On the other hand, the ability of THF to completely suppress the coordination of Me_2N-group to the exophilic metal centers of **3** provides an additional means of selectivity regulation.

2-Allyl-4-halogene-1-methoxybenzenes **4r-s** isomerize quantitatively in 5 min, no signs of dehydrobenzene formation due to activation of α-CH bonds next to the halogen were detected. The strong electron withdrawing effect of the two *m*-CF_3 groups leads to a slowdown of the isomerization, which takes 100 h to complete at room temperature. 2-Allyl-4-X-1-methoxybenzenes (X = $SiMe_3$ (**4u**); Ph_2P (**4v**)) also perform excellent selectivity and high yields, however total conversions require 100 h at room temperature.

A set of allylbenzenes containing protected functional groups (**4w**-**y**) were evaluated as shown in Scheme 2. MOM-protection of the hydroxy group proved to be suitable, and the reaction of **4w** proceeded selectively without decomposition of the ester group. The substrates with dioxolane- and 2,2'-dimethylimidazoline-protected *p*-carbonyl and *m*-carboxyl groups also smoothly underwent C=C bond transposition, however for **4x** and **4y** a noticeable drop of reaction rates was documented.

Several allyl-functionalized heterocycles, including thiophene (**4z**), N-methyl carbazole (**4za**), 8-methoxyquinoline (**4zb**), 2-pyrazolylpyridine (**4zc**) were converted into the desired products with 96-97% *E*-content. The corresponding *E*-propenyl derivatives have potential as building blocks for biologically active molecules. Importantly we successfully extended this methodology to substrates containing two allyl groups in aryl and heteroaryl moieties, demonstrating further underscoring the versatility and synthetic potential of this transformation.

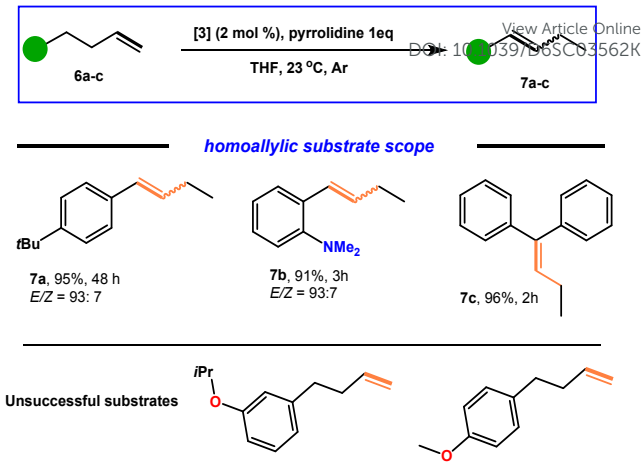

Scheme 3. Isomerization of homoallylbenzenes **6a-c** catalyzed by complex **3.**

In the case of 3,6-diallyl-N-methylcarbazole (**4za**) and 2,6-diallylanisole (**4zd**), both allyl groups isomerize with equal efficiency.

Next, we investigated the possibility to transpose a remote double-bond in homoallyl benzenes (Scheme 3). For but-3-en-1-ylbenzene derivatives, the displacement of the double bond across two bonds proved to be feasible under the same conditions. For homoallylbenzenes **6a**-**c**, the double bond was found to move exclusively at the position conjugated with the aromatic ring. It is obvious that a powerful driving force of the "chain walking" process over one position is styrene formation, where the double bond is conjugated with aryl moiety. Substrates with *para*- and *ortho*-substituted aryls, as well as but-3-ene-1,1-diyldibenzene, readily undergo isomerization within 2 to 48 hours.

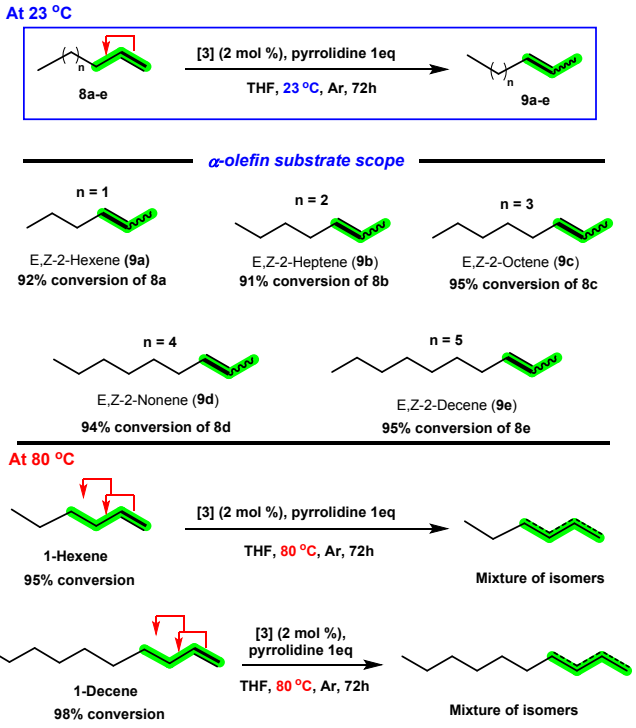

Scheme 4. Isomerization of α-olefins **8a-e** catalyzed by complex **3.**

View Article Online
DOI: 10.1039/D6SC03562K

ARTICLE

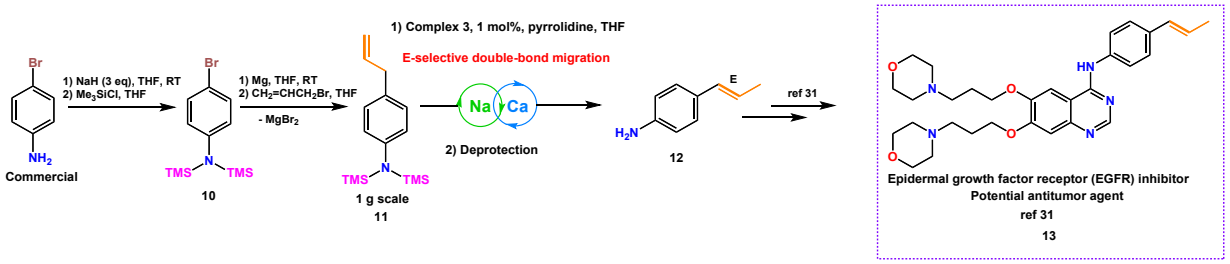

Scheme 5. Gram-scale preparation of *p*-(*E*)-propenylaniline building block.

Unfortunately, unlike allylbenzenes, homoallylbenzene substrates bearing an isopropyl- and methyl- protected hydroxyl functionality does not isomerize. Even in the presence of 10 mol% of complex **3**, no evidence for C=C bond transposition was detected. Increasing the temperature to 80 °C also does not give the desired effect.

Isomerization of α-olefins produced by petroleum processing on the million-ton scale into their internal congeners is of high importance for industrial applications, particularly in the production of plasticizers and detergent alcohols as well as other valuable products. The absence of any activating substituents in α-olefins (aryl, RO-, R_2N- etc), providing the thermodynamic driving forces that dictate the translocation of the C=C bond, makes achieving the necessary regioselectivity of the process extremely challenging. A C=C bond "chain walking" process in α-olefins still remains difficult to realize even under catalysis by precious metal complexes.[3b, 29]

The selective mono-isomerization of terminal alkenes into 2-alkenes has received increased attention, and Fe-, Ni- and, especially, Co-based catalysts have mainly succeeded.[6a, 7a, 14a, 30] However, even the use of supporting intricate ligands and organometallic co-catalysts, previously reported "alkene zipper" complexes, does not solve the problem of achieving high conversions and selectivity in α-olefin isomerization.

To our delight, complex **3** was found to enable the transposition of a C=C bond (at 23 °C) in a series of α-olefins from 1-hexene to 1-decene. A remarkable feature of this reaction is the selective C=C bond migration to position 2 of related terminal alkene with 93% regioselectivity, albeit without stereoselectivity. Compared to the isomerization of allylbenzenes, a much longer reaction time of 72 h is required to achieve optimal yields (91-95%). The occurrence of a regioselective reaction not provided by conjugation with aryls, as in the case of allyl and homoallylbenzenes, is very interesting. In broad contrast, the sodium superbase NaTMP described in 2024, catalyzes the isomerization of 1-octene, to afford a mixture of regioisomers.[17b] Most likely, the mono-isomerization of α-olefins catalyzed by heterobimetallic complex **3** is kinetically controlled. Indeed, the regioselectivity of the isomerization process proved to be sensitive to temperature.

Thus, isomerization of 1-hexene and 1-decene at 80 °C results in the formation of a mixture of regioisomers.

An increase in temperature to 100 °C and reaction time does not allow for shifting the equilibrium towards the single regioisomer formation.

Synthetic Application

The protocol engaging catalysis by complex **3** offers new opportunities for development of preparative routes of the production of a variety of important biologically active molecules, including potential drugs without the use of toxic transition metals. To evaluate the synthetic applicability of the catalytic approach we developed, the synthesis of *p*-*E*-propenylaniline (**12**) in 1 gram-scale was performed. This compound elaborated in 2017 as an epidermal growth factor receptor (EGFR) inhibitor (**13**) exhibited outstanding antitumor activity (Scheme 5).[31] We proposed an alternative transition metal free approach to propenylaniline in which the key step of the synthesis is the stereoselective isomerization of TMS-protected allylaniline **11**. The target *p*-*E*-propenylaniline **12** was synthesized in two stages from cheap commercially available *p*-bromoaniline. As shown in scheme 5, the isomerization reaction of 12 mmol of allylaniline **11** in the presence of 1 mol% of complex **3** proceeds smoothly and completes in 2 h. After completion of the isomerization and facile deprotection of amino group, the desired *E*-propenylaniline was isolated by flash distillation as an oil with a final yield of 87% and 96% *E*-selectivity.

Mechanistic Studies and DFT calculations

It is logical to assume that the heterobimetallic amide complex $[(C_4H_8N)_3Ca]Na$ (**14**) is the likely genuine catalytic species for the above mentioned olefin isomerizations (Scheme 6). Indeed, as it was evidenced by ^1H NMR spectroscopy the reaction of **3** with excess pyrrolidine leads to protonolysis of all M-C bonds, disappearance of the complex and the formation of free $(p\text{-}tBuC_6H_4)_2CH_2$ (SI, Fig. S67). The new heterobimetallic

View Article Online
DOI: 10.1039/D6SC02562H

amide complex **14** was detected due to the appearance in the ^{1}H NMR spectrum of the reaction mixture of broadened singlets at 2.93 and 1.56 ppm corresponding to the *α*- and *β*-protons of the pyrrolidinide fragments.

These signals are downfield shifted relative to the protons of free pyrrolidine (2.61 and 1.39 ppm in C_6D_6).[21] In the $^{13}C\{^1H\}$ NMR spectrum, the corresponding carbons appear as broadened singlets at 49.76 and 26.47 ppm. To evaluate the aggregation of **14** in solution, ^{1}H DOSY NMR spectrum was recorded in C_6D_6 in the presence of (*m*,*m*-$tBu_2C_6H_3)_2CH_2$, (*p*-$tBuC_6H_4)_2CH_2$ and Me_4Si as internal standards (SI, Fig. S69). In the absence of donor solvent, the complex proved to be monomeric and to represent a contact ion pair similarly to the published heterobimetallic amide complex {$[(Me_3Si)_2N]_3Ca$}Li.[32]

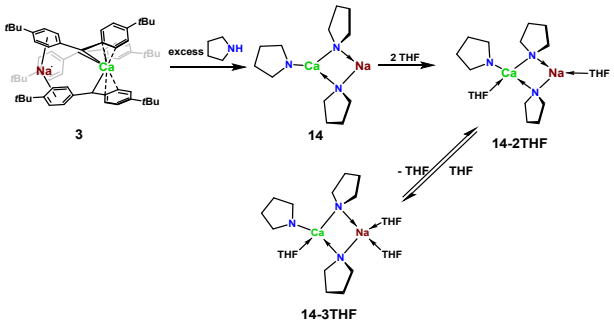

Scheme 6. Formation of catalytically active heterobimetallic amide complex $[(C_4H_8N)_3Ca]Na$ (**14**).

The molecular mass (FW = 269.15 g/mol^{-1}) extracted from the spectrum corresponds to the one expected for the formula $[(C_4H_8N)_3Ca]Na$ (SI, Fig. S70). Unfortunately, all attempts to obtain X-ray suitable single crystals of complex **14** were unsuccessful.

The coordination of pyrrolidinide anions with Ca and Na cations does not ensure the coordination saturation of their spheres in **14**. Since the catalysis was performed in THF, most likely this issue is fixed by coordinating THF molecules. To model this, possible structures with 2 to 7 THF molecules (SI, Scheme S1) were calculated at the r^2-SCAN-3c/Def2-TZVP,CPCM(THF) level (DFT calculation details presented in SI). The r^2-SCAN-3c functional was chosen based on its versatility, accuracy and high performance, which has been confirmed everywhere.[33] Calculations of their formation energies (SI, Table S2) show that the addition of 2 or 3 THF molecules is relatively favourable, i.e., one THF molecule coordinated to Na and one to Ca is sufficient to stabilize **14**. Consequently, the catalytically active complex is present as **14-2THF** or **14-3THF** (Scheme 6), probably being in equilibrium. Both retain the ability to coordinate an alkene, which is expected to be stronger in the case of **14-2THF** (SI, Table S3).

Possible mechanisms and the catalytic cycles were calculated at the r^2-SCAN-3c/Def2-TZVP,CPCM(THF) level (Scheme 7). The catalytic reaction can proceed *via* alkene coordination to Na (**CM1**) or Ca (**CM2**) ion. Subsequently CH_2 group of the coordinated alkene can be deprotonated either by the terminal nitrogen atom N_t (Path **CM1-t** or **CM2**) or the bridging nitrogen N_{br} (Path **CM1-br**), since they feature identical negative QTAIM charges of –1.23 ē.

After alkene coordination to Ca (Path **CM2**), proton transfer to N_{br} becomes less favourable due to the significant distance between N_{br} and the CH_2 group (over 4 Å); therefore, only path **CM2** involving proton transfer to N_t was considered. It should be noted that the stereochemical direction of the reaction (*E*/*Z* isomerism of product **5**) is determined at the stage of alkene **4** coordination to **14-2THF**, but the difference between **CM1** and **CM2** at this stage (intermediates **PS1**) is minor. Thus, six possible pathways for the isomerization of **4a** (Ar = Ph) leading to *E*-**5a** and *Z*-**5a** were considered. The corresponding energy diagram and energetic parameters are presented in Figures 3, S164, S165 and Table S4.

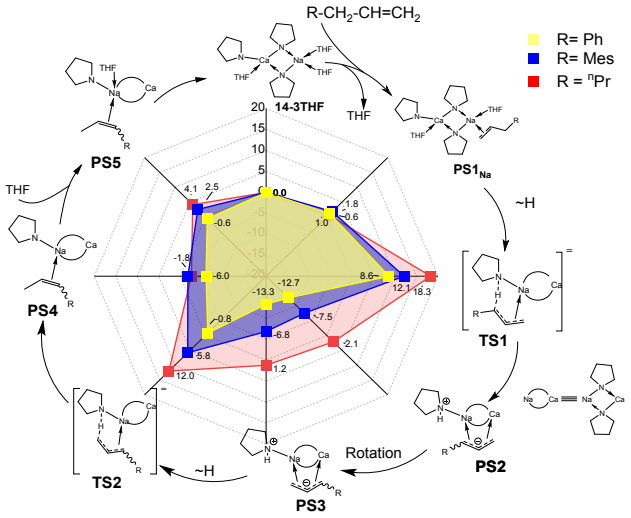

Figure 3. Energetic ΔG^o_{298} (kcal/mol) circular diagram for the reaction **14-3THF** with **4a** (*yellow*), **4e** (*blue*), and **8a** (*red*) *via* path **CM1-t** calculated at the r^2-SCAN-3c/Def2-TZVP,CPCM(THF) level. The energetic diagram in classical linear view presented in Fig. S165.

Analysis of the energetic profile of the catalytic isomerization cycle for **4a** (Table S4) reveals that the energies of the least stable intermediates (**PS1**) do not exceed 8 kcal/mol, and the barriers for CH_2 group deprotonation (**TS1**) and allylic fragment protonation (**TS2**) are not high. In particular, the ΔG^a_{298} values ranging from 7.6 to 17.3 kcal/mol for proton transfer indicate a fast process. Overall, there is qualitative agreement with experimental observations that the reactions are quite fast. The circular diagram in Figure S164 in SI allows for visual identification of the most energetically favourable catalytic process based on the minimal polygon area. This is the mechanism **CM1-t** leading to *E*-**5a** (yellow in Fig. 3 and Fig. S164), i.e., *via* alkene coordination to Na centre and CH_2 deprotonation by the terminal pyrrolidinide.

View Article Online
DOI: 10.1039/D6SC03562K

ARTICLE

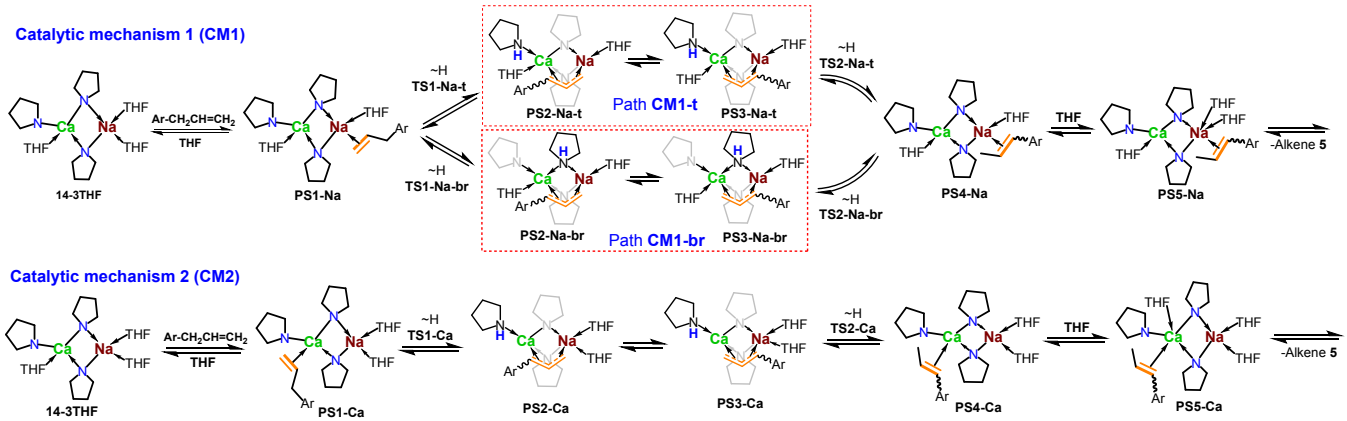

Scheme 7. Proposed mechanisms for catalytic cycle.

The lower preference for **CM2** *via* calcium is also indicated by the relative stability of **14-2THF(B)** (SI, Scheme S1), which is 8.4 kcal/mol less stable than **14-2THF**, determining the effective barrier for the **PS1$_{Ca}$** and **PS1$_{Na}$** formation stages, respectively.

A distinctive feature of the mechanisms involving coordination to Na (mechanism **CM1-t** and **CM1-br**) is the structure of the allylic intermediates **PS2** and **PS3**, for which a topological analysis of the electron density in frames of the theory "Atoms in molecules» (QTAIM)[34] was performed (the obtained parameters for the most important interactions are presented in Table S4, molecular graphs are shown at Fig. 4 and S166, S167, and S169. QTAIM graph reveals bond critical point (BCP) (3;-1) (red circles) and corresponding bond paths (green lines) for all covalent bonds and also for weak noncovalent interactions with metals. In particular, two BCP (3;-1) and bond paths between carbon atoms of allyl and metals exhibit (Fig. 4), therefore the allylic fragment in *E*,*Z*-**PS2$_{Na}$** and *E*,*Z*-**PS3$_{Na}$** interacts with both Na and Ca simultaneously.

The strength of the Na…C and Ca…C contacts estimated via standart correlation of potential energy density V(r) (see description in ESI) at corresponding BCP varies in the ranges of 1.6–3.8 and 2.2–5.2 kcal/mol (Table S6), respectively, providing additional stabilization. Thus, the structure of the **PS2$_{Na}$** and **PS3$_{Na}$** intermediates causes a synergistic effect of the catalytic activity of the bimetallic complex **14.**

The *Z*-**PS2** and *Z*-**PS3** intermediates leading to *Z*-**5a** are less stable compared to those for *E*-**5a** across all mechanisms (their energies are on average 2.5 kcal/mol higher, while the maximum value reaches 5.7 kcal/mol). Meanwhile they have similar activation barriers (the difference of 1.1 to 4.5 kcal/mol for proton transfer is insignificant, Table S6). Thus, the DFT calculations confirm that the formation of *E*-**5a** is thermodynamically and kinetically more favourable than that of *Z*-**5a**.

To rationalize the stereoselectivity of the isomerization reactions for substrates **4e** and **4f** with sterically hindered Ar-groups, which yield a significant amount of the *Z*-isomer, thermodynamic parameters for the reaction **4** → *E*,*Z*-**5** with all aryl substituents were calculated (Table S6). For Ar = Mes (**4e**), energetic parameters *via* mechanisms **CM1-t** and **CM1-br** were estimated (Table S7). The obtained values show that *Z*-**5e** is more stable than *E*-**5e** by ΔG°_{298} = 1.9 kcal/mol, which is caused by the trivial steric effect lifting effective conjugation between the C=C bond and the benzene ring in *E*-**5e**. The energetic parameters for the isomerization of **4e** *via* mechanisms **CM1-t** and **CM1-br** (corresponding diagram in Fig. S166) show that the most preferred mechanism is *E*-**CM1-t**, namely, the formation of *E*-**5e** is slightly more kinetically favourable. The kinetic effect is determined by the higher stability of the *E*-allylic intermediates compared to the *Z*-isomeric ones (difference ΔG°_{298} of 7.3 and 9.7 kcal/mol for *E*,*Z*-**PS2$_{Na}$-t(e)** and *E*,*Z*-**PS3$_{Na}$-t(e)**, respectively), whereas the thermodynamic effect has an opposite action since *Z*-**5e** is more stable by ~2 kcal/mol. Therefore, the competition between these weak and stereochemically opposite kinetic (slightly predominant) and thermodynamic effects explains the *E*-**5e** : *Z*-**5e** ratio close to 2:1 (Scheme 7). A similar relationship of effects can be extended to the case of **5f**.

The effect of the substrate type was elucidated using the DFT calculations as well, in particular the energy diagram at Fig. 1 compares the reactions of **4a**, **4e**, and **8a**. The polygon area of this circular diagram decreases in the order **8a** (^{n}Pr) > **4e** (Mes) > **4a** (Ph), which expectedly indicates the lowest reactivity in the series for the non-activated 1-hexene (**8a**). This is primarily caused by the substantially less stable allylic intermediates *E*-

PS2$_{Na}$(8a) and *E*-**PS3$_{Na}$(8a)**, for which the $\Delta G°_{298}$ values are positive (SI, Table S9), unlike the analogous values for *E*-**PS2$_{Na}$(a)**, *E*-**PS3$_{Na}$(a)**, *E*-**PS2$_{Na}$(e)**, *E*-**PS3$_{Na}$(e)** (Tables S5 and S7). A benzene ring and its conjugation with the allylic moiety in *E*-**PS2$_{Na}$(8a)** and *E*-**PS3$_{Na}$(8a)** is absent, even though coordination to both metals is still present (QTAIM data for **8a** are given in Table S10 and Fig. S168 in SI). The second decelerating factor for **8a**, albeit minor due to possible proton tunnelling, is the noticeably higher barrier (ΔG^{a}_{298} = 17.7 kcal/mol) for the deprotonation stage of **8a**, while for **4a** and **4e** the analogous activation energies are 10 kcal/mol or less.

Using DFT calculations, we also explained the regioselectivity of isomerization of non-activated alkenes **8**. For this purpose, the energetic parameters for the stepwise isomerization of **8a** to 2-hexene (**9a**) and then to 3-hexene (**9a'**) were calculated (Fig. 5, Fig. S170, Table S9). Thermodynamically, **9a** and **9a'** differ insignificantly (the isomerisation $\Delta G°_{298}$ values are –3.0 and –2.5 kcal/mol, respectively), but it should be noted that the formation of **9a** is faster than that of **9a'**, albeit not much and only due to the lower stability of the intermediates *E*-**PS2$_{Na}$(9a)** and *E*-**PS3$_{Na}$(9a)** by 1.7 and 2.8 kcal/mol, respectively. Therefore, an increase in temperature leads to a mixture of isomeric hexenes.

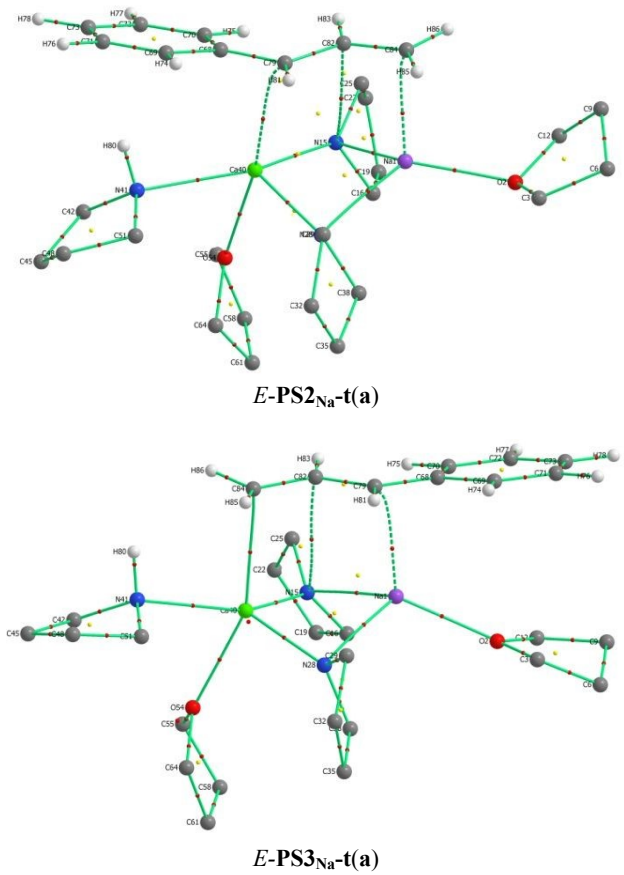

Figure 4. QTAIM-molecular graphs for the most stable allylic-intermediates *E*-**PS2$_{Na}$-t(a)** and *E*-**PS3$_{Na}$-t(a)**, corresponding QTAIM parameters are presented in Table S4. Hydrogens of CH_2 and weak C…H and H…H interactions are omitted for clarity. Small red circles are bond critical points (3;-1), small yellow circles are ring critical points (3;+1), green lines are bond paths.

Thus, the performed DFT calculations of the catalytic isomerization of **4a**, **4e**, and **8a** showed that the preferred mechanism is the process in which the alkene coordinates to the sodium ion of the catalytically active bimetallic complex (**14-3THF**), followed by proton transfer to the nitrogen atom of the terminal pyrrolidinide group (**CM1-t**). In the resulting allylic intermediates, coordination to both metal centres occurs (Fig. 4), which causes a synergistic effect on the catalytic activity of the Ca-Na catalyst studied. The reaction barriers and relative stabilities of all intermediates fall within a sufficiently narrow range of [–14; +19] kcal/mol, which is consistent with the fast reaction rates. Kinetically, the formation of the *E*-isomer is more favourable even for the sterically hindered substrate **4e** (Ar = Mes). For the latter, the *Z*-isomer is thermodynamically more favourable, which explains the resulting mixture of *E*,*Z*-isomers of alkene **5e**. For nonactivated 1-hexene (**8a**), the reaction is predicted to proceed at a slower rate in general; however, 2-hexene (**9a**) formation is slightly faster than 3-hexene (**9a'**).

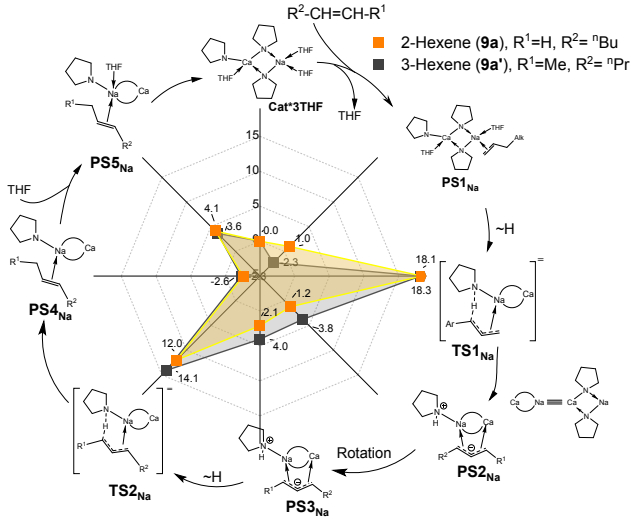

Figure 5. Energetic $\Delta G°_{298}$ (kcal/mol) circular diagram for the catalytic isomerization of 1-hexene (**8a**) (*orange*) and 2-hexene (**9a**) (*black*) via path **CM1-t** calculated at the r^2-SCAN-3c/Def2-TZVP,CPCM(THF) level. The energetic diagram in classical linear view presented in Fig. S170.

Conclusions

Herein we report on the synthesis and structure of cheap and readily available base-free heterobimetallic tris(benzhydryl) sodium calciate {[(*p*-*t*Bu-C$_6$H$_4$)$_2$CH]$_3$Ca}Na which performed unprecedented catalytic activity in the isomerization of terminal olefins. Isomerizations of allyl- and homoallylbenzenes occur under thermodynamic and kinetic

control, leading to the formation of conjugated systems with high *E*-selectivity (up to 98%); excluding sterically demanding substrates **4e**,**f**. Isomerization of α-olefins from 1-hexene to 1-decene, catalyzed by complex **3**, at room temperature proceeds under kinetic control and yields 2-olefins (as a mixture of *E*- and *Z*-stereoisomers) with up to 93% regioselectivity. The mechanistic studies revealed that the genuine catalyst for isomerization is a heterobimetallic amide complex $[(C_4H_8N)_3Ca]Na$ (**14**) characterized in solution by ^1H, $^{13}C\{^1H\}$ and ^1H DOSY NMR studies. DFT calculations of catalytic mechanisms elucidate kinetic and thermodynamic control for different types of substrates and explain *E*/*Z*-regioselectivity. The high efficiency of catalyst **3** can be attributed to the synergistic effect of two metals in formed catalytically active complex **14**, as demonstrated by QTAIM analysis. In particular, the stability of allylbenzene intermediates can be additionally increased by coordinating them with both metallic centers of **14** up to ~5 kcal/mol. The elaborated approach was shown to be readily upscaled and successfully applied for the synthesis of gram amounts of 2-*E*-olefins.

Author contributions

A. N. S. and A. A. T. conceived and directed the project. I. V. K. performed synthetic experiments. A. V. C. performed X-ray analysis. R. R. A. performed DFT calculations. A. N. S. and A. A. T. wrote the manuscript with assistance from all authors.

Conflicts of interest

The authors declare no competing financial interests.

Data availability

The Supporting Information is available free of charge on the RCS Publications website and includes Experimental Section, characterization data, NMR spectra of new compounds, DFT and crystallographic information (PDF), optimized Cartesian coordinates (XYZ). Deposition Numbers 2469412 (**1**), 2469413 (**2**), and 2469414 (**3**) contain the supplementary crystallographic data for this paper. These data can be obtained free of charge via the joint Cambridge Crystallographic Data Centre (CCDC).

Acknowledgements

The financial support of the Russian Science Foundation is highly acknowledged (Project No. 23-73-10148). The SC XRD data were obtained using the equipment of the Center for Collective Use "Analytical Centre of the IOMC RAS". This work was performed employing the equipment of the Centre for Collective Use of IOMC RAS. DFT calculations were performed using the equipment of the Centre for Collective Use of INEOS RAS.

References

View Article Online
DOI: 10.1039/D6SC03562K

1 (a) K. Itami and J. Yoshida, *Bull. Chem. Soc. Jpn*., 2006, **79**, 811; (b) N. Armanino, J. Charpentier, F. Flachsmann, A. Goeke, M. Liniger and P. Kraft, *Angew. Chem. Int. Ed*., 2020, **59**, 16310.

2 (a) E. Larionov, H. Li and C. Mazet, *Chem. Commun*., 2014, **50**, 9816; (b) G. Hilt, *ChemCatChem*., 2014, **6**, 2484; (c) M. Hassam, A. Taher, G. E. Arnott, I. R. Green and W. A. L. van Otterlo, *Chem. Rev*., 2015, **115**, 5462; (d) J. J. Molloy, T. Morack and R. Gilmour, *Angew. Chem. Int. Ed*., 2019, **58**, 13654; (e) D. Fiorito, S. Scaringi and C. Mazet, *Chem. Soc. Rev*., 2021, **50**, 1391; (f) S. Zhang and M. Findlater, *Synthesis*, 2021, **53**, 2787; (g) X. Liu, Q. Liu, X. Liu, and Q. Liu, *Chem Catalysis*, 2022, **2**, 2852; (h) A. H. Obeid and J. Hannedouche, *Adv. Synth. Catal*., 2023, **365**, 1100; (i) T. M. Trnka and R. H. Grubbs, *Acc. Chem. Res*., 2001, **34**, 18; (j) R. R. Schrock and A. H. Hoveyda, *Angew. Chem. Int. Ed*., 2003, **42**, 4592; (k) B. J. Gregori, M. W. S. Schmotz and A. J. von Wangelin, *ChemCatChem*, 2022, **14**, e202200886; (l) R. Kusy and K. Grela, *Chem. Rev*. 2025, **125**, 4397.

3 (a) D. Gauthier, A. T. Lindhardt, E. P. K. Olsen, J. Overgaard and T. Skrydstrup, *J. Am. Chem. Soc.,* 2010, **132**, 7998; (b) A. L. Kocen, K. Klimovica, M. Brookhart and O. Daugulis, *Organometallics*, 2017, **36**, 787; (c) S. L. Kraus, S. P. Ross and M. S. Sigman, *Org. Lett*., 2021, **23**, 2505.

4 (a) S. M. M. Knapp, S. E. Shaner, D. Kim, D. Y. Shopov, J. A. Tendler, D. M. Pudalov and A. R. Chianese, *Organometallics,* 2014, **33**, 473; (b) M. R. Kita and A. J. M. Miller, *Angew. Chem. Int. Ed*., 2017, **56**, 5498; (c) S. De-Botton, O. A. Filippov, E. S. Shubina, N. V. Belkova and D. Gelman, *ChemCatChem.,* 2020, **12**, 5959.

5 S. Scaringi and C. Mazet, *ACS Catal*., 2021, **11**, 7970.

6 (a) C. Chen, T. R. Dugan, W. W. Brennessel, D. J. Weix and P. L. Holland, *J. Am. Chem. Soc*., 2014, **136**, 945; (b) S. Zhang, D. Bedi, L. Cheng, D. K. Unruh, G. Li and M. Findlater, *J. Am. Chem. Soc*., 2020, **142**, 8910; (c) J. Zhao, B. Cheng, C. Chen and Z. Lu, *Org. Lett*., 2020, **22**, 837.

7 (a) R. Jennerjahn, R. Jackstell, I. Piras, R. Franke, H. Jiao, M. Bauer and M. Beller, *ChemSusChem*., 2012, **5**, 734; (b) X. Yu, H. Zhao, P. Li and M. J. Koh, *J. Am. Chem. Soc*., 2020, **142**, 18223; (c) S. Garhwal, A. Kaushansky, N. Fridman and G. de. Ruiter, *Chem Catalysis*, 2021, **1**, 631.

8 R. Castro-Rodrigo, S. Chakraborty, L. Munjanja, W. W. Brennessel and W. D. Jones, *Organometallics*, 2016, **35**, 3124.

9 W. Yang, I. Yu. Chernyshov, M. Weber, E. A. Pidko and G. A. Filonenko, *ACS Catal*., 2022, **12**, 10818.

10 C. Z. Rubel, A. K. Ravn, H. C. Ho, S. Yang, Zi-Q. Li, K. M. Engle and J. C. *Angew. Chem. Int. Ed*., 2024, **63**, e202320081.

11 J. Zhong, X. Wang, M. Luo and X. Zeng, *Org. Lett*., 2024, **26**, 3124.

12 (a) S. Biswas, *Comments Inorg. Chem*., 2015, **35**, 300; (b) T. Kobayashi, H. Yorimitsu and K. Oshima, *Chem. Asian J*., 2009, **4**, 1078; (c) E. H. P. Tan, G. C. Lloyd-Jones, J. N. Harvey, A. J. J. Lennox and B. M. Mills, *Angew. Chem. Int. Ed*., 2011, **50**, 9602; (d) C. R. Larsen and D. B. Grotjahn, *J. Am. Chem. Soc*., 2012, **134**, 10357; (e) T. C. Cao, A. L. Cooksy and D. B. Grotjahn, *ACS Catal*., 2020, **10**, 15250; (f) E. Bergamaschi, F. Beltran and C. J. Teskey, *Chem. Eur. J*., 2020, **26**, 5180; (g) S. A. Lutz, A. K. Hickey, Y. Gao, C.-H. Chen and J. M. *J. Am. Chem. Soc*., 2020, **142**, 15527; (h) C. R. Woof, D. J. Durand, N. Fey, E. Richards and R. L. Webster, *Chem. Eur. J.,* 2021, **27**, 5972; (i) D. Kim, G. Pillon, D. J. DiPrimio and P. L. Holland, *J. Am. Chem. Soc*., 2021, **143**, 3070; (j) S. Sanz-Navarro, M. Mon, A. Doménech-Carbó, R. Greco, J. Sánchez-Quesada, E. Espinós-Ferri and A. Leyva-Pérez, *Nat. Commun*., 2022, **13**,

2831; (k) T. C. Jankins, C. Z. Rubel, H. C. Ho, R. Martin-Montero, K. M. Engle, *Chem. Sci*., 2025, **16**, 2307.
13 (a) A. Kapat, T. Sperger, S. Guven and F. Schoenebeck, *Science*, 2019, **363**, 391; (b) M. Tricoire, D. Wang, T. Rajeshkumar, L. Maron, G. Danoun and G. Nocton, *JACS Au*., 2022, **2**, 1881; (c) L. Huang, E. Q. Lim and M. J. Koh, *Chem Catalysis.,* 2022, **2**, 508.
14 (a) Q.-Y. Meng, T. E. Schirmer, K. Katou and B. König, *Angew. Chem. Int. Ed*., 2019, **58**, 5723; (b) S. Gnaim, A. Bauer, H.-J. Zhang, L. Chen, C. Gannett, C. A. Malapit, D. E. Hill, D. Vogt, T. Tang, R. A. Daley, W. Hao, R. Zeng, M. Quertenmont, W. D. Beck, E. Kandahari, J. C. Vantourout, P.-G. Echeverria, H. D. Abruna, D. G. Blackmond, S. D. Minteer, S. E. Reisman, M. S. Sigman and P. S. Baran, *Nature*, 2022, **605**, 687; (c) V. Palani and A. E. Wendlandt, *J. Am. Chem. Soc*., 2023, **145**, 20053; (d) X. Song, Y.-Q. Huang, B. Zhao, H. Wu, X. Qi and J. Wang, *J. Am. Chem. Soc*., 2025, **147**, 20644; (e) M. Dong, S. Jia, X. Chen, J. Jiao, C. Xue, Z. Xia, H. Cheng, T. Deng, C. Chen, K. Dong, H. Wu, M. He and B. Han, *J. Am. Chem. Soc*., 2025, **147**, 19976.
15 (a) G. Occhialini, V. Palani, and A. E. Wendlandt, *J. Am. Chem. Soc*., 2022, **144**, 145; (b) A. Messara, B. Kweon, F. Woge, C. G. Daniliuc, C. Mück-Lichtenfeld and R. Gilmour, *J. Am. Chem. Soc*., 2025, **147**, 36677; (c) R. Manikandan, R. S. Phatake and N. G. Lemcoff, *Chem. Eur. J*., 2022, **28**, e202200634; (d) T. Morack, C. Onneken, H. Nakakohara, C. Mück-Lichtenfeld and R. Gilmour, *ACS Catal*., 2021, **11**, 11929; L. Blank and R. Gilmour, *ACS Catal*. 2026, **16**, 4125.
16 D. J. Cram and R. T. Uyeda, *J. Am. Chem. Soc*., 1964, **86**, 5466.
17 (a) R. F. Algera, Y. Ma and D. B. Collum, *J. Am. Chem. Soc*., 2017, **139**, 11544; (b) A. Tortajada, G. L. Righetti, A. McGinley, M. Mu, M. Garcia-Melchor and E. Hevia, *Angew. Chem. Int. Ed*., 2024, **63**, e202407262; (c) S.-J. Lou, P. Wang, X. Wen, A. Mishra, X. Cong, Q. Zhuo, K. An, M. Nishiura, Y. Luo and Z. Hou, *J. Am. Chem. Soc*., 2024, **146**, 26766; (d) H. M. H. Martinez, S. M. Hampton, S. R. Isbel, C. N. MacFarlane, E. B. Aparicio, E. A. Ble-Gonzalez and A. Bugarin, *ACS Omega,* 2026, **11**, 18419; (e) F. Krämer, T. M. H. Downie and R. E. Mulvey, *Angew. Chem. Int. Ed*., 2026, **65**, e23460.
18 (a) A. M. Camp, M. R. Kita, P. T. Blackburn, H. M. Dodge, C.-H. Chen and A. J. M. Miller, *J. Am. Chem. Soc*., 2021, **143**, 2792; (b) A. S. Chang, M. A. Kascoutas, Q. P. Valentine, K. I. How, R. M. Thomas and A. K. Cook, *J. Am. Chem. Soc*., 2024, **146**, 15596.
19 (a) S. D. Robertson, M. Uzelac and R. E. Mulvey, *Chem. Rev*., 2019, **119**, 8332; (b) L. Davin, A. H. Gomez, C. McLaughlin, A. R. Kennedy, R. McLellan, E. Hevia, *Dalton Trans.,* 2019, **48**, 8122; (c) C. Glock, H. Gorls and M. Westerhausen, *Chem. Commun.,* 2012, **48**, 7094.
20 (a) A. N. Selikhov, G. S. Plankin, A. V. Cherkasov, A. S. Shavyrin, E. Louyriac, L. Maron and A. A. Trifonov, *Inorg. Chem*., 2019, **58**, 5325; (b) A. N. Selikhov, A. S. Shavyrin, A. V. Cherkasov, G. K. Fukin and A. A. Trifonov, *Organometallics,* 2019, **38**, 4615; (c) A. N. Selikhov, E. N. Boronin, A. V. Cherkasov, G. K. Fukin, A. S. Shavyrin and A. A. Trifonov, *Adv. Synth. Catal*., 2020, **362**, 5432; (d) A. N. Selikhov, I. V. Lapshin, A. V. Cherkasov, G. K. Fukin and A. A. Trifonov, *Organometallics*, 2021, **40**, 3042; (e) A. N. Selikhov, A. V. Cherkasov, Y. V. Nelyubina and A. A. Trifonov, *Mendeleev Commun*., 2021, **31**, 334; (f) A. N. Selikhov, A. V. Cherkasov, K. A. Lyssenko and A. A. Trifonov, *Organometallics,* 2022, **41**, 820; (g) V. A. Kirkina, A. A. Kissel, A. N. Selikhov, Y. V. Nelyubina, O. A. Filippov, N. V. Belkova, A. A. Trifonov and E. S. Shubina, *Chem. Commun*., 2022, **58**, 859.
21 A. N. Selikhov, A. V. Cherkasov, Y. V. Nelyubina and A. A. Trifonov, *ACS Catal*., 2023, **13**, 12582.
22 L. Lochmann, J. Pospišil and D. Lim, *Tetrahedron Lett*., 1966, **7**, 257.
23 D. Li, I. Keresztes, R. Hopson and P. G. Williard, *Acc. Chem. Res*., 2009, **42**, 270.
24 M. A. Guino-o, C. F. Campana and K. Ruhlandt-Senge, *Chem. Commun*., 2008, 1692.
25 F. G. Bordwell, *Acc. Chem. Res*., 1988, **21**, 456.
26 (a) A. N. Selikhov, Y. V. Nelyubina, R. R. Aysin and A. A. Trifonov, *Dalton Trans*., 2025, **54**, 4503; (b) M. A. Bogachev, A. N. Selikhov, A. V. Cherkasov, R. R. Aysin, S. S. Bukalov and A. A. Trifonov, *J. Am. Chem. Soc*., 2025, **147**, 34610.
27 X.-Yu. Zhang, L. Zheng and B.-T. Guan, *Org. Lett*., 2018, **20**, 7177.
28 E. Vitaku, D. T. Smith and J. T. Njardarson, *J. Med. Chem*., 2014, **57**, 10257.
29 (a) C. R. Larsen, G. Erdogan and D. B. Grotjahn, *J. Am. Chem. Soc*., 2014, **136**, 1226; (b) Y. Wang, C. Qin, X. Jia, X. Leng and Z. Huang, *Angew. Chem. Int. Ed*., 2017, **56**, 1614.
30 (a) T. Kobayashi, H. Yorimitsu and K. Oshima, *Chem. As. J*., 2009, **4**, 1078; (b) S. W. M. Crossley, F. Barabe and R. A. Shenvi, *J. Am. Chem. Soc*., 2014, **136**, 16788; (c) A. Schmidt, A. R. Nödling and G. Hilt, *Angew. Chem. Int. Ed*., 2015, **54**, 801; (d) F. Weber, A. Schmidt, P. Röse, M. Fischer, O. Burghaus and G. Hilt, *Org. Lett*., 2015, **17**, 2952; (e) X. Liu, W. Zhang, Y. Wang, Z.-X. Zhang, L. Jiao and Q. Liu, *J. Am. Chem. Soc*., 2018, **140**, 6873.
31 L. Chen, Y. Zhang, J. Liu, W. Wang, X. Li, L. Zhao, W. Wang and B. Li, *Eur. J. Med. Chem*., 2017, **138**, 689.
32 A. R. Kennedy, R. E. Mulvey and R. B. Rowlings, *J. Organomet. Chem*., 2002, **648**, 288.
33 S. Grimme, A. Hansen, S. Ehlert, and J.-M. Mewes, *Chem. Phys.*, 2021, **154**, 64-103.
34 R. F. W. Bader, Atoms in Molecules: A Quantum Theory, Oxford Univ. Press, Oxford, **1990**.

View Article Online
DOI: 10.1039/D6SC03562K

The data supporting this article, including NMR spectra, IR spectra, crystal data and structure refinement details, DFT-calculations have been included as part of the Supplementary Information. See DOI: https://doi.org.....

The crystallographic data for **1**-**3** have been deposited with the Cambridge Crystallographic Data Centre (CCDC no. 2469412-2469414). These data can be obtained free of charge via http://www.ccdc.cam.ac.uk/structures/